

We are IntechOpen, the world's leading publisher of Open Access books Built by scientists, for scientists

6,900

Open access books available

185,000

International authors and editors

200M

Downloads

Our authors are among the

154

Countries delivered to

TOP 1%

most cited scientists

12.2%

Contributors from top 500 universities



WEB OF SCIENCE™

Selection of our books indexed in the Book Citation Index
in Web of Science™ Core Collection (BKCI)

Interested in publishing with us?
Contact book.department@intechopen.com

Numbers displayed above are based on latest data collected.
For more information visit www.intechopen.com



Structural Insights from Recent CB1 X-Ray Crystal Structures

Rufaida Al-Zoubi, Dow P. Hurst and
Patricia H. Reggio

Additional information is available at the end of the chapter

<http://dx.doi.org/10.5772/intechopen.80783>

Abstract

Over the past 2 years, X-ray crystal structures of the antagonist- and agonist-bound CB1 receptor have been reported. Such structures are expected to accelerate progress in the understanding of CB1 and should provide an exceptional starting point for structure-based drug discovery. This chapter examines the consistency of these X-ray structures with the CB1 experimental literature, including mutation, NMR and covalent labeling studies. These comparisons reveal discrepancies between this literature and the TMH1-2-3 region of each CB1 crystal structure. The chapter also examines crystal packing issues with each X-ray structure and shows that the discrepancies with the experimental literature can be attributed to crystal packing problems that force the N-terminus deep in the binding pocket of the two inactive state structures and force TMH2 to bend at G2.53/S2.54 and invade the binding pocket in the activated state structure. Revision is advisable before these structures are used for structure-based drug discovery.

Keywords: cannabinoid CB1 receptor, CB1 mutation, CB1 cross-linking, CB1 nuclear magnetic resonance, crystal packing

1. Introduction

The cannabinoid receptor type 1 (CB1) belongs to the G-protein coupled receptors (GPCRs) superfamily. GPCRs comprise the largest group of integral membrane proteins that mediate cellular responses to a wide spectrum of signaling molecules including peptides, lipids, neurotransmitters, glycoproteins, as well as light, taste and odor substances. They act via coupling and activating intracellular effector proteins including G-proteins and arrestins leading to an array of intracellular signaling cascades.

GPCRs have a common architecture of seven transmembrane helices (TMHs) joined by extracellular (EC) and intracellular (IC) loops of varied lengths, in addition to an extracellularly extending N terminus, and an intracellular C terminus that begins with an amphipathic alpha helical segment (Helix 8) oriented parallel to the cell membrane. In Class A GPCRs, the binding site for the endogenous ligand is generally formed by the EC core within the TMH bundle, and may extend to EC loops, referred to as the orthosteric binding site. Ligands may also bind to distinct (allosteric) binding sites in the receptor.

Due to the various physiological functions mediated by GPCRs, they are considered major targets for drug discovery and design of novel therapeutics. However, understanding the structure-function relationship of these proteins and the design of high affinity, selective ligands that target these receptors requires a detailed knowledge of the three-dimensional structure of the receptor in general and of the ligand binding site in specific. However, structural characterization for membrane proteins in general has been a challenge due to their low expression in recombinant hosts and their inherent instability in surfactants. It was not until the year 2000 that the first high resolution GPCR structure was resolved by X-ray crystallography, Rhodopsin in its inactive state [1]. The following 10 years witnessed the release of other inactive state crystal structures of class A GPCRs (e.g. the Adenosine A2A, and the $\beta 1$ and $\beta 2$ adrenergic receptors [2–4]), in addition to the release of the active state crystal structure of Rhodopsin in complex with a synthetic peptide resembling the C-terminus of the G-alpha subunit of transducing [5]. Available structures during that time served as templates for homology modeling for other GPCRs including the CB1 receptor. And parallel with biophysical studies, available crystal structures provided structural insights for their activation mechanism. A breakthrough in GPCR structural characterization has been achieved in the last 8 years with more than 200 structures for different GPCRs being deposited in the Protein Data Bank, including the CB1 inactive and active state crystal structures which have been resolved in 2016, and in 2017 respectively [6–8]. Before that, structural characterization of CB1 orthosteric as well as allosteric binding domains have been extensively studied via mutations, site-directed labeling, mass spectrometry, SAR studies, and in-silico methods, and will be discussed in detail throughout this chapter.

2. Structural divergence of the cannabinoid receptors from class A GPCRs

The CB1 receptor is a class A (Rhodopsin-like) GPCR (**Figure 1**). Different phylogenetic studies and multidimensional scaling analysis of Class A GPCRs classify cannabinoid receptors (CB1/CB2) into one cluster along with the endothelial differentiation G-protein coupled receptors (EDGRs) (including Sphingosine 1-phosphate receptors (S1P) and Lysophosphatidic acid receptors (LPA)) [9–12]. Receptors from those families, except for the LPA_{4/6}, share common sequence divergence from other Class A GPCRs. Specifically, the absence of helix kinking proline residues in TMH2 and TMH5, and the absence of a disulfide bridge between the EC-2 loop and C3.25 at the EC end of TMH3. Instead, they share an internal disulfide bridge in the EC-2 loop, a conserved PxxGW motif at the EC end of TMH4, in addition to a Y5.39 that forms an aromatic pi-pi stack with W4.64 in that motif resulting in a similar shape of the EC2 loop as seen in the crystal structures for the CB1, S1P₁, and LPA₁ receptors [6, 7, 13, 14]. At the

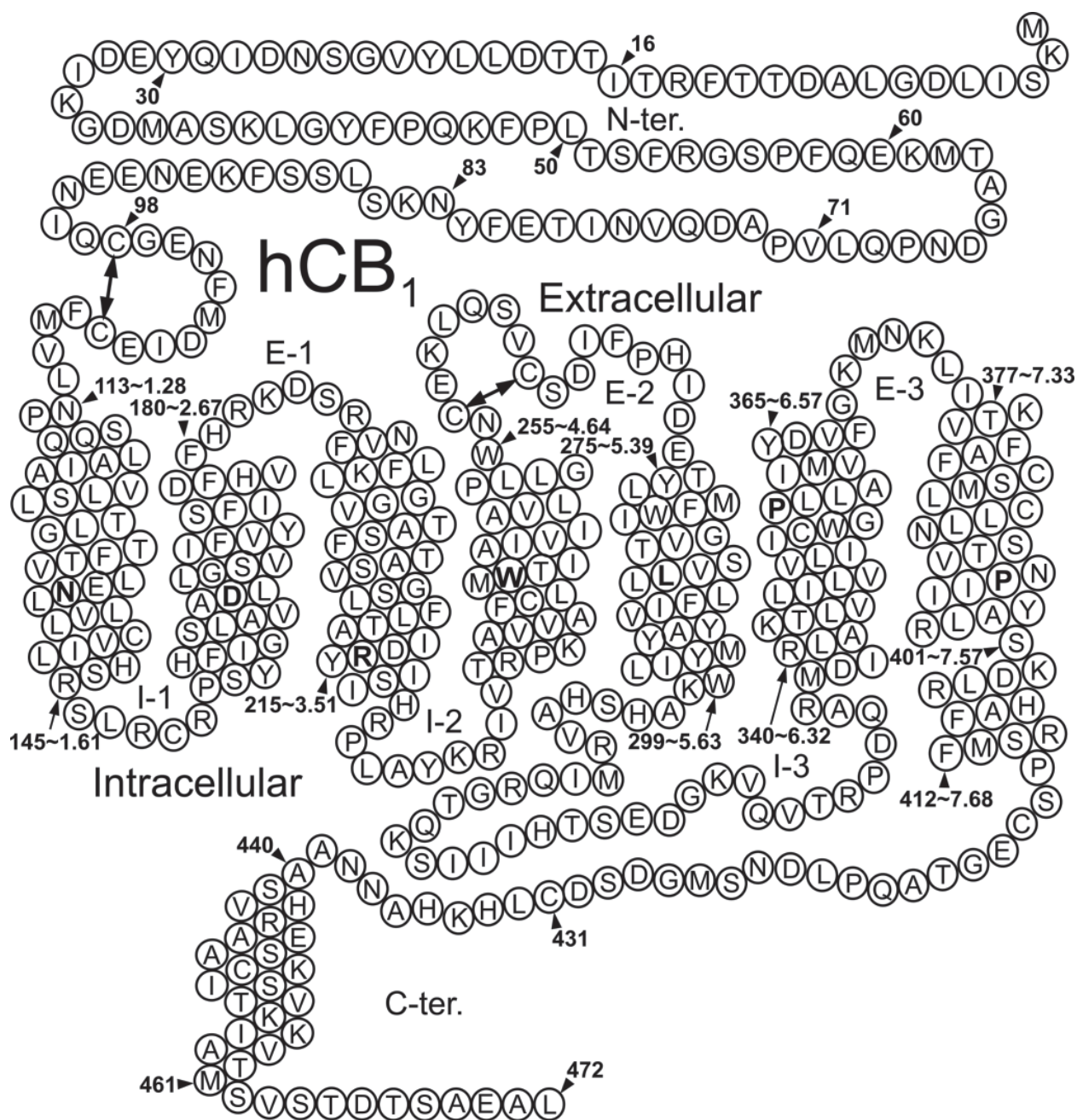


Figure 1. Helix net representation of the hCB₁ receptor. The most highly conserved residue in each helix is shown in bold. Residues are numbered using the BW#: Ballesteros-Weinstein residue numbering system in GPCRs which uses the X.YY format; X denotes the transmembrane helix number and (YY) denotes residue position relative to the most conserved residue in the helix (X.50). Loop regions are numbered using absolute sequence numbers.

binding site, they share a common basic residue (K/R 3.28) on TMH3 and an aromatic residue (F/Y 2.57) on TMH2. In addition, the S1P receptors are like CB1/CB2 in the presence of E1.49 at TMH1. E1.49 has been reported to be a key interaction site for pregnenolone (an endogenous negative allosteric modulator that protects the brain from *cannabis* intoxication) with CB1 [15], while the LPA₁₋₃ receptors share a W5.43 with CB1/CB2 that has been shown to affect antagonist binding to the cannabinoid receptors [16]. In addition, S1P₁, and the cannabinoid receptors recognize lipid-derived ligands that have been shown to bind to the receptor by diffusing from bulk lipid towards the binding site via a transmembrane portal [6, 7, 14, 17, 18].

3. CB1 receptor crystal structures

Two inactive state crystal structures for the hCB1 receptor have been resolved. The first structure (PDB ID: 5TGZ) was resolved at 2.8 Å; the receptor was truncated at both the N-terminus (1–98) and the C-terminus (415–472), with a flavodoxin protein fused into the IC3 loop (V306, P332), the receptor was crystalized in complex with a biaryl-pyrazole derivative (AM6358, **Figure 2**) and using thermo-stabilizing mutations (T3.46A, E5.37K, T5.47V, and R6.32E) [6]. The second structure was resolved at 2.6 Å (PDB ID: 5U09) in complex with an acyclic high affinity inverse agonist of the CB1 receptor, taranabant (**Figure 2**) [7]. In this structure, fewer amino acid residues were truncated from the N-terminus (1–76) and the C-terminus (422–472), and *P. abysii* glycogen synthase protein was fused into the IC3 loop (A301, D333) of a single point mutant (T3.46A) hCB1 receptor [7]. In both structures, resolved residues were from E100 at the N-terminus to F412 at the C-terminus of the receptor.

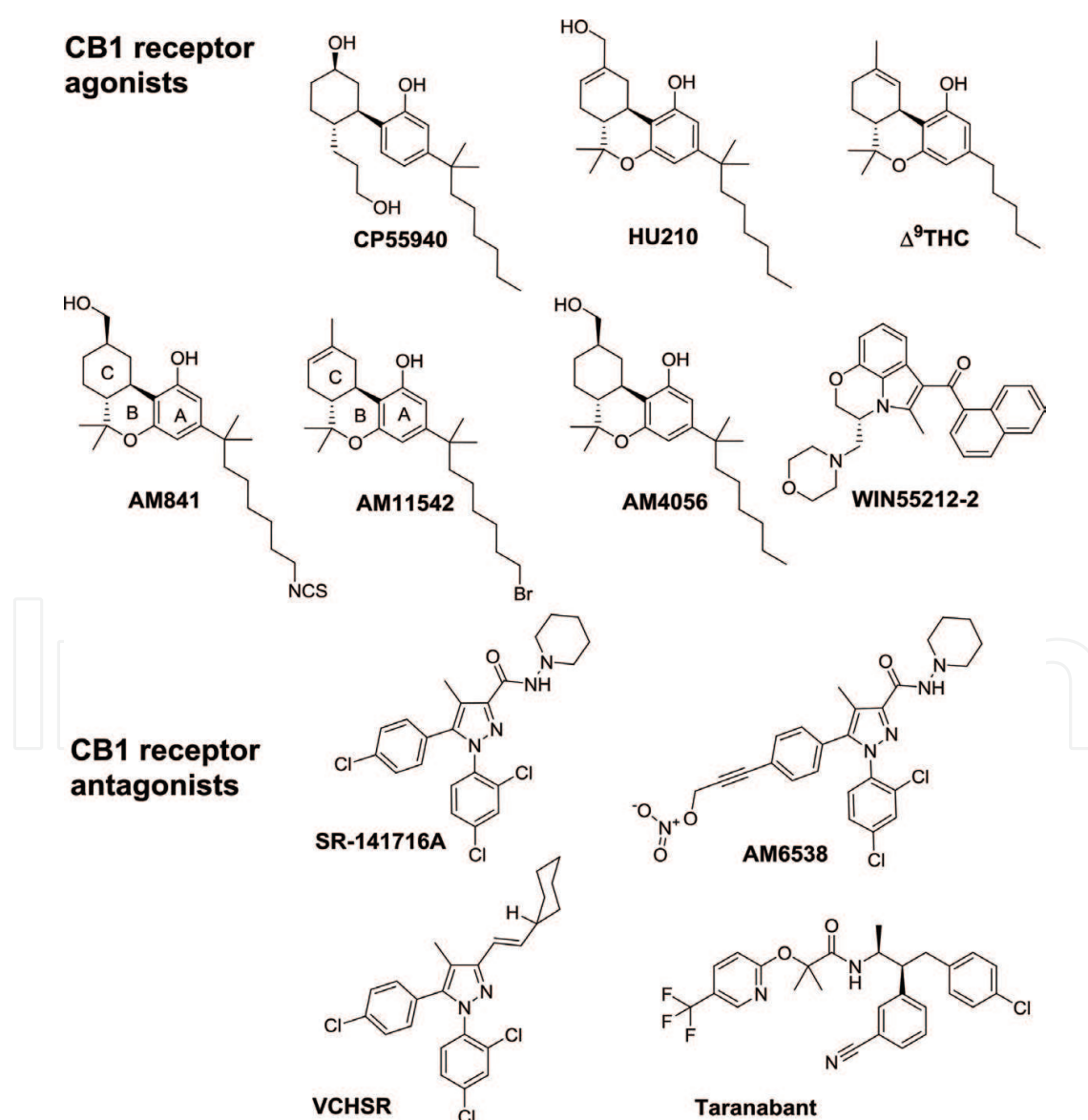


Figure 2. Compounds discussed in this chapter.

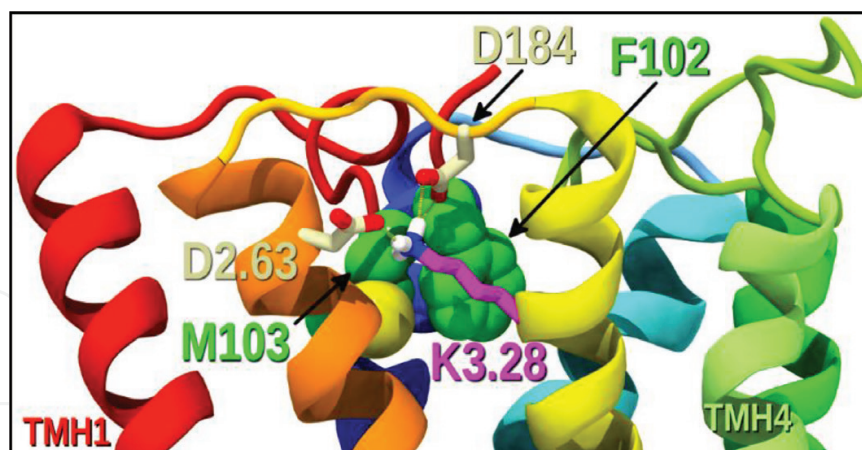


Figure 3. N-terminus residues F102 and M103 (green VdW) penetrate the binding crevice in the inactive state CB1 structure (PDB ID: 5U09). This influences the positions of K3.28 (magenta tube), D2.63 and D184 (wheat tube) which form an interaction with each other.

Agonist bound hCB1 crystal structures (PDB IDs: 5XRA, 5XR8) were resolved at 2.80 and 2.95 Å resolution and in complex with the classical cannabinoids (AM11542, AM841) respectively (**Figure 2**). The receptor was constructed in a similar way to the AM6358-bound crystal structure. Resolved residues included D104-S414 and F102-S414 in the 2.80 and 2.95 Å resolution structures respectively [8].

Inactive state CB1 structures show a transmembrane portal for antagonist entry between TMH1 and TMH7 that is similar to the S1P₁ structure. However, the membrane proximal region in the CB1 receptor forms a loop that extends towards the orthosteric binding site with two amino acid residues (F102, M103) invading unpredictably the binding site in the inactive state structures and forming Van der Waal (VDW) interactions with the antagonists (**Figure 3**) [6, 7].

Active state structures show characteristic conformational changes featuring class A GPCR activation including an outward movement and a counterclockwise rotation (EC view) of the IC end of TMH6, resulting in a break in the R3.50/D6.30 inactive state “ionic lock” [19, 20]. Unlike inactive state structures, a transmembrane portal is not present in active state structures due to the packing of the EC domain of TMH1 towards TMH7. In addition, the N-terminus resides at the top of the receptor with no invasion of the orthosteric binding site. On the other hand, the active state binding site displays a profound (53%) reduction in size that is resulting from an inward kink of the EC domain of TMH2 towards the orthosteric binding site, as well as, rotation of TMH3 towards TMH2 [8].

4. Mutation and labeling studies on CB1: consistency with CB1 crystal structures

Multiple mutation studies on either mCB1 or hCB1 were aimed to study the receptor’s binding site and to identify key residues for CB1 receptor activation (**Figure 4**). While different ligands were used in functional and binding affinity assessment, WIN55212, SR141716A and CP55940, were used primarily, due to the availability of tritiated versions of these compounds.

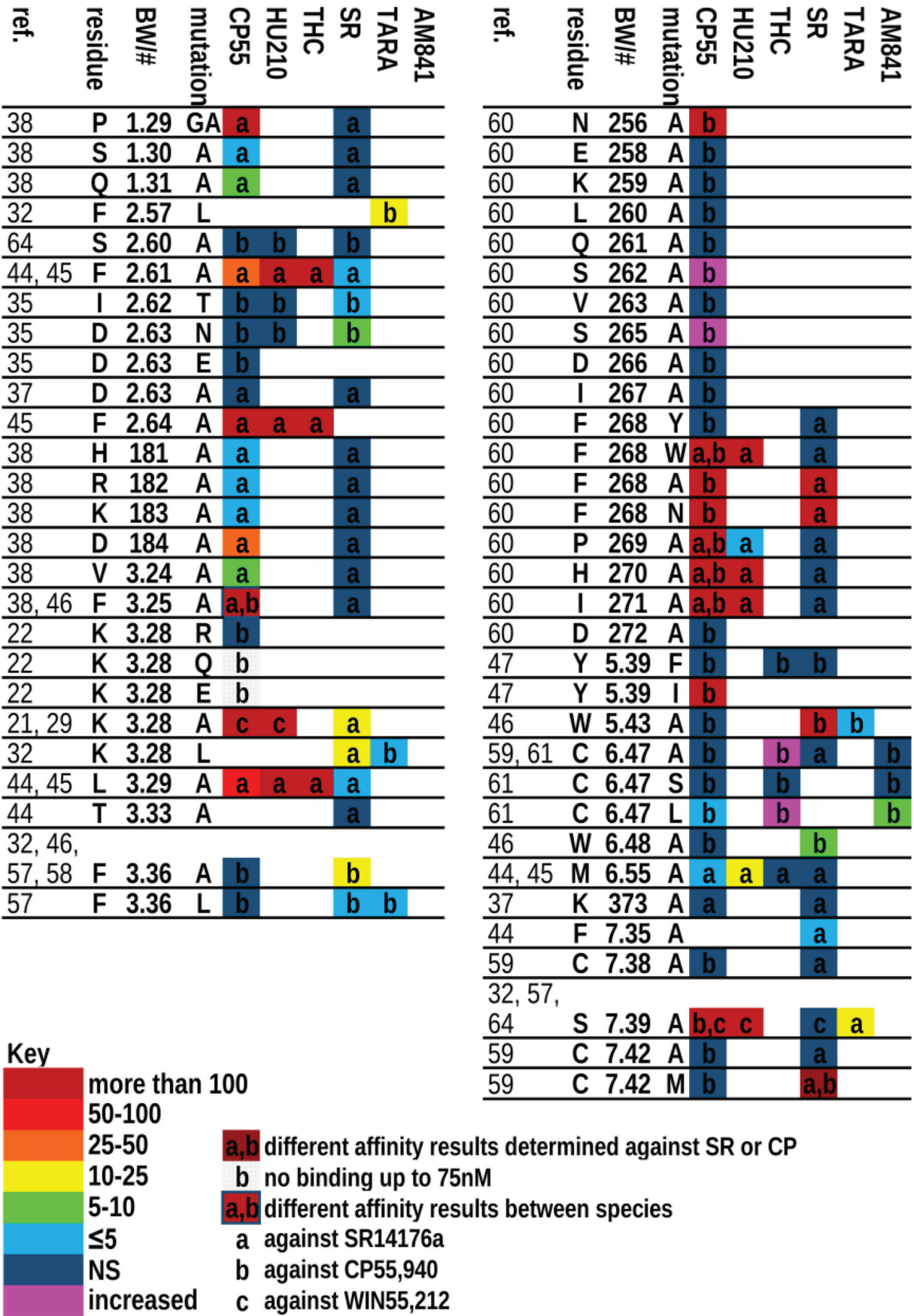


Figure 4. Mutations in or near the binding crevice of the CB1 receptor. The key represents changes in binding affinities of ligands to mutant CB1 receptor compared to WT. Residues are numbered using Ballesteros-Weinstein numbers. See Figure 1 for more details.

Other ligands characterized include HU210, Δ^9 -THC, taranabant, and AM251. The discussion here will be focused on mutation and labeling studies near the orthosteric binding site and those affecting crystalized ligands or closely related structures such as SR141716A, HU201, or CP55940 (**Figure 2**).

4.1. K3.28 residue

One of the earliest mutational studies on the CB1 receptor targeted K3.28 [21, 22]. The lipophilic nature of CB1 ligands and the fact that the third TMH in CB1 has a V3.32 instead of an acidic residue at that position (as being conserved in aminergic receptors), directed the attention towards K3.28 to investigate its role in ligand binding.

Song and Bonner first reported that the binding of CP55940, HU210, and anandamide to a K3.28A mutant hCB1 expressed in HEK293 cells resulted in severe impairment, with more than 100-fold decrease in their potencies in inhibiting cAMP accumulation. On the other hand, the binding and the potency of WIN55212 at the K3.28A mutant receptor were comparable to WT, suggesting that the receptor is still functioning [21]. Shortly afterwards, Kendall's Lab demonstrated retained binding affinity and potency for CP55940 in CHO cells expressing K3.28R hCB1 mutant, with no binding for up to 75 nM concentration in cells expressing K3.28Q or K3.28E mutants compared to cells expressing WT receptor ($K_d = 7.7 \pm 3.5$ nM). In the same study, WIN55212 displayed comparable affinity for the three mutants with more than one order of magnitude decrease in potency in the K3.28E mutant, while its potency in K3.28Q mutant was not determined due to low receptor density [22]. A significant loss of CP55940's potency in stimulating [35 S]GTP γ S binding in HEK293 cells expressing the K3.28A hCB1 mutant were also reported where the EC_{50} values for the WT and the mutant receptor were 1.3 and 225 nM respectively [23].

Results suggested that the loss of potencies of anandamide, and the classical and non-classical cannabinoids, but not WIN55212 at the K3.28A mutant is due to their low affinities to the receptor, and a basic residue at 3.28 is required for CP55940 binding. Based on mutation data, modeling studies suggested a hydrogen bond interaction between K3.28 and the amide oxygen of anandamide [16, 24], and with classical and non-classical cannabinoids [25–27]. While Shim argued later that K3.28 is important for stabilizing the binding site for the endocannabinoids and the classical and non-classical cannabinoids and not directly involved in their binding [28].

K3.28 mutations have also been demonstrated to affect affinities and deactivation profile of biaryl-pyrazole derivatives. The affinity of SR141716A to K3.28A hCB1 mutant has been reported to be 17-fold lower compared to the WT [29]. In addition, SR141716A was reported to act as neutral antagonist with loss of ability to turn off receptor's basal activity in inhibiting Ca^{2+} currents in SCG neurons microinjected with K3.28A hCB1 mutant cDNA [30]. This data prompted a mutant cycle study using an SR141716A analog (VCHSR) to test the hypothesis that an interaction between the carboxamide oxygen in SR141716A and K3.28 is essential for its inverse agonist activity. The results supported the hypothesis by demonstrating that VCHSR acts as neutral antagonist with comparable affinities to both K3.28A and WT receptor [29]. A set of SR141716A analogues were also designed later that support the hypothesis [31]. A K3.28L mutation at hCB1 has been also reported to lower the binding affinity of AM251 by 17-fold compared to the WT, while it had no effect on the affinity of the acyclic antagonist, taranabant, to the receptor [32]. The discriminatory effect of K3.28 mutants on different classes

of antagonists may suggest different binding interactions within the receptor's binding site, especially that taranabant acts also as an inverse agonist [33].

CB1 crystal structures, on the other hand, do not support proposed hydrogen bonding of ligands to K3.28. In both inactive state and the active state structures of CB1, K3.28 orients its side chain towards the TMH2/3 interface forming salt bridges with D184 in the EC1 loop and D2.63 at the top of TMH2. The K3.28/D2.63 interaction is only noticeable in the inactive state crystal structures (**Figure 3**).

4.2. D2.63 mutations

As described above, this residue forms a salt bridge with K3.28 in the inactive state crystal structures (**Figure 4**). This K3.28/D2.63 salt bridge has been previously proposed to be essential for CB1 basal activity [34]. However, an earlier study on K3.28A mutant reported a comparable basal activity to the WT receptor in inhibiting Ca^{2+} currents which does not support the role of K3.28/D2.63 salt bridge in controlling receptor's basal activity [30]. Individual effects of D2.63 mutation on ligand binding and receptor activation have been also reported. In HEK293 cells expressing a D2.63N hCB1 mutant, binding affinities for the classical cannabinoid (HU210), non-classical cannabinoid (CP55940), and the amino alkyl indole (WIN55212) were not significantly different from WT, while the affinity for SR141716A was 5-fold decreased compared to the WT. In addition, the potencies of CP55940 and HU210 in stimulating [^{35}S] GTP γ S binding were significantly different from WT with about 12-fold increase in their EC_{50} values, while the basal activity of the D2.63N mutant was not different from WT [35]. In a different study, a double hCB1 mutant (L3.43A/D2.63A) was shown to lower the affinity of CP55940 to the receptor by 7-fold, while increasing the affinity of SR141716A by 3-fold. The L3.43A single mutant had an opposite effect by increasing the affinity of CP55940 to the receptor by 6-fold and lowering the affinity of SR141716A by 7-fold. Knowing that L3.43A mutation has been shown to increase the basal signaling of CB1 receptor in stimulating [^{35}S] GTP γ S binding, combining D2.63A with L3.43A mutation lowered the basal signaling below CB1 WT levels. Results suggest that D2.63 may be involved in receptor activation and that mutation into alanine stabilizes the inactive state of the receptor [34, 36]. A modeling and mutation study suggested that an ionic interaction between D2.63 and K373 in the EC-3 loop is important for receptor activation. In the study, a reciprocal mutant D2.63K/K373D resulted in similar potencies for CP55940 and WIN55212 in stimulation for [^{35}S]GTP γ S compared to the WT receptor, while their potencies were more than 5-fold lower in the single and double alanine mutants [37]. Such an interaction is not present in the crystal structures.

4.3. Mutation studies on the CB1 N-terminus

The CB1 receptor is unique in having a relatively long (114 amino-acid residues) N-terminus compared to other class A GPCRs. Analysis of the amino acid sequence of the membrane proximal region (MPR) of the amino terminus reveals a remarkably high degree of conservation in that region (**Figure 5**).

Early studies on the N-terminus reported no effect on prolylglycine insertion in the N-terminus (at A73, L86, and E100) of hCB1 receptor expressed in HEK 293T cells on agonist (CP55940) and antagonist (SR141716A) binding. In addition, S1.30A and Q1.31A mutants at the N-terminal

UniProt ID	Species		
SP O02777 CNR1_FELCA	Felis catus (Cat)	M K S I L D G L A D T T F R T I	16
SP P21554 CNR1_HUMAN	Homo sapiens (Human)	M K S I L D G L A D T T F R T I	16
SP Q333S9 CNR1_PELES	Pelophylax esculentus (Edible frog)	M K S V L D G L A D T T F R T I	16
SP P47746 CNR1_MOUSE	Mus musculus (Mouse)	M K S I L D G L A D T T F R T I	16
SP Q801M1 CNR1_XENLA	Xenopus laevis (African clawed frog)	M K S I L D G L A D T T F R T I	16
SP Q71SP5 CNR1_MACMU	Macaca mulatta (Rhesus macaque)	M K S I L D G L A D T T F R T I	16
SP Q5IS73 CNR1_PANTR	Pan troglodytes (Chimpanzee)	M K S I L D G L A D T T F R T I	16
SP P20272 CNR1_RAT	Rattus norvegicus (Rat)	M K S I L D G L A D T T F R T I	16
SP P56971 CNR1_TAEGU	Taeniopygia guttata (Zebra finch)	M K S I L D G L A D T T F R T I	16
TR G5E6R9 G5E6R9_BOVIN	Bos taurus (Bovine)	M K S I L D G L A D T T F R T I	16
SP Q9PUI7 CNR1_TARGR	Taricha granulosa (Roughskin newt)	M K S I L D G L A D T T F R T I	16

Cat	T T D L L Y V G S N D I Q Y E D I K G D M A S K L G Y F P Q K F P	49
Human	T T D L L Y V G S N D I Q Y E D I K G D M A S K L G Y F P Q K F P	49
Edible Frog	T T D L L Y M G P N E V Q Y E D T K S D L - S K L G Y Y P Q K L P	48
Mouse	T T D L L Y V G S N D I Q Y E D I K G D M A S K L G Y F P Q K F P	49
African clawed frog	T T D L L Y L G P N E V Q Y D D S K G D I S S K L V Y F P Q K L P	49
Rhesus macaque	T T D L L Y V G S N D I Q Y E D I K G D M A S K L G Y F P Q K F P	49
Chimpanzee	T T D L L Y V G S N D I Q Y E D I K G D M A S K L G Y F P Q K F P	49
Rat	T T D L L Y V G S N D I Q Y E D I K G D M A S K L G Y F P Q K F P	49
Zebra finch	T T D L L Y V G S N D I Q Y E D M K G D M A S K L G Y Y P Q K F P	49
Bovine	T T D L L Y M G A N D I Q Y E D I K S D M A S K L G Y F P Q K F P	49
Roughskin newt	T T D L L Y M G S N D V Q Y E D T K G E M A S K L G Y F P Q K L P	49

Cat	L T S F R G S P F Q E K M T A G D N S Q L V - - P A - D Q V N I T	79
Human	L T S F R G S P F Q E K M T A G D N P Q L V - - P A - D Q V N I T	79
Edible Frog	L S S Y - - - - Q E K I I - - D G - Q S T L - H L - D S F N A T	71
Mouse	L T S F R G S P F Q E K M T A G D N S P L V - - P A G D T T N I T	80
African clawed frog	L S S L R G D P L H E K M T I I D D P L L S I - P - L D Q I N A T	80
Rhesus macaque	L T S F R G S P F Q E K M T A G D N P Q L V - - P A - D Q V N I T	79
Chimpanzee	L T S F R G S P F Q E K M T A G D N P Q L V - - P A - D Q V N I T	79
Rat	L T S F R G S P F Q E K M T A G D N S P L V - - P A G D T T N I T	80
Zebra finch	L S S F R G D P F Q E K M T G G D D S L L S I I P S - E Q V N I T	81
Bovine	L T S F R G S P F Q E K M T A G D S P Q L V - - P A - D Q V N L T	79
Roughskin newt	L S S F R R D H S P D K M T I G D D N L L S F Y P L - D Q F N V T	81

Cat	E F Y N K S L S S Y K E N E E N I Q C G E N F M D M E C F M I L N	112
Human	E F Y N K S L S S F K E N E E N I Q C G E N F M D I E C F M V L N	112
Edible Frog	E F Y N K S I T T F K D G D G N I Q C G N N F M D M E C F M I L T	104
Mouse	E F Y N K S L S S F K E N E D N I Q C G E N F M D M E C F M I L N	113
African clawed frog	D F Y N K S I - I F K D T D D N V Q C G K N F M D M E C F M I L T	113
Rhesus macaque	E F Y N K S L S S F K E N E E N I Q C G E N F M D I E C F M V L N	112
Chimpanzee	E F Y N K S L S S F K E N E E N I Q C G E N F M D I E C F M V L N	112
Rat	E F Y N K S L S S F K E N E E N I Q C G E N F M D M E C F M I L N	113
Zebra finch	E F Y N K S L S T F K D N E E N I Q C G E N F M D M E C F M I L N	114
Bovine	E F Y N K S L S S Y K E N D E N I Q C G E N F M D M E C F M I L N	112
Roughskin newt	E F F N R S V S T F K E N D D N L K C G E N F M D M E C F M I L T	114

Key	Highly Conserved	Charge Conserved	S/T Conserved
	Conserved	Internal disulfide	Beta Branch I/V/T

Figure 5. Sequence alignment of the CB1 N-terminus of 11 different species downloaded from the UniProt online database (www.uniprot.org).

end of TMH1 did not affect the binding affinity for SR141716A, while they reduced the binding affinity of CP55940 by 5- and 10-fold respectively [38].

In addition, CP55940 binding to truncated receptor at the N-terminal region ($\Delta 64$, $\Delta 80$, $\Delta 89$, $\Delta 103$ shCB1) was comparable to the WT receptor [39, 40]. On the other hand, the binding affinity of SR141716A to the $\Delta 103$ synthetic hCB1 (shCB1) truncation mutant was higher compared to the WT with retained ability to inhibit basal signaling of the truncated mutant [39]. As described earlier, in the (inactive state CB1 X-ray crystal structures, two amino acid residues from the N-terminus occupy the receptor's orthosteric binding site, forming strong VDW interactions with the antagonists, those are F102, M103. Affinity data of SR141716A to the $\Delta 103$ shCB1 truncation mutant is inconsistent with the inactive state crystal structures.

Reduction of the proposed disulfide bridge at the N-terminus C98/C107 reduces CP55940 potency in [^{35}S]GTP γ S binding assay [39]. However, a previous study reported that a double mutant of the two cysteine residues into serine subtly affected CP55940 binding, but did not affect SR141716A binding [41]. It is worth-mentioning that the C98/C107 residues are conserved among all 11-CB1 species available from UniProt. This sulfide bridge is not apparent in crystal structures.

Interestingly, a recent mutational, and modeling study from the Kunos lab identified an N-terminal residue (M106 in rodent CB1 compared to I105 in hCB1) as the determinant of the species differential affinity of {5-(4-chlorophenyl)-N-[(1R,2R)-2-hydroxycyclohexyl]-6-(2-methoxyethoxy)-3-pyridinecarboxamide} (14 h) at the CB1 receptor [42]. The compound, has been described previously as a peripherally selective, high affinity CB1 receptor antagonist [43]. However, this compound has been shown to have higher affinity for the hCB1 receptor compared to mouse and rat CB1 receptor [42]. This residue faces the ligand binding site in crystal structures, but with a changed position in the different structures.

4.4. EC1 loop

Mutations of the EC1 loop negatively impacted CP55940 but not SR141716A binding, the K_i value of CP55940 was 26-fold higher in D184A hCB1 mutant compared to the WT receptor expressed in HEK293 cells. Here, the K_i was determined by competition binding against [^3H]SR141716A [38]. This aspartate residue forms an ionic interaction with K3.28 in both the active and inactive state CB1 crystal structures (**Figure 3**) [6–8]. H181A, R182A, and K183A have also lowered CP55940 affinity by 3–4-fold compared with the WT [38]. None of the EC1 loop residues forms direct contact with crystallized ligands.

4.5. Aromatic residues lining the orthosteric binding site

The orthosteric binding site of CB1 is lined with multiple aromatic residues located on TMH2/3/5/6/7, as well as, F286 in the EC2 loop.

4.5.1. F2.57, F2.61, and F2.64

F2.57 is two turns extracellular to the conserved D2.50, facing the orthosteric binding site. In the inactive state CB1 crystal structures, this residue has been shown to form an aromatic

π - π stack with the 2,4-dichlorophenyl ring in AM6538 [6], and with the cyanophenyl ring in taranabant [7]. Mutation data show a reduced affinity for taranabant and AM251 (a diarylpyrazole antagonist) by 30- and 97-fold respectively in F2.57L hCB1 mutant [32]. In addition, both SR141716A and AM6538 failed to antagonize 100 nM CP55940-induced inhibition of cAMP in F2.57A hCB1 mutant while preserving their abilities in F2.57W hCB1 mutant [6]. Results indicate a major role for this residue in antagonist binding via aromatic interactions and in shaping the antagonist binding site. On the other hand, while this residue shows a major contact with the agonists (A-ring, **Figure 2**) in the AM11542 and the AM841 bound crystal structures, [8] CP55940 displayed similar potency for inhibition of cAMP in both F2.57A, and F2.57W mutants compared to WT [8].

Mutations on F2.61 revealed effects on antagonist and agonist binding and potencies. In the inactive state CB1 structures, this residue is rotated towards TMH1 and its side chain is at the TMH1/TMH2 interface, yet it forms moderate VDW interactions with the piperidine and with the trifluoro-methyl pyridine in AM6538 and taranabant respectively [6, 7]. While in the active state structures, this residue faces the binding site and forms strong VDW interactions with the agonists (AM11542 and AM841) B-ring (**Figure 2**) [8]. SR141716A displayed only 5-fold higher K_d value in F2.61A hCB1 mutant transiently expressed in HEK293 cells [44], but both SR141716A and AM6538 failed to antagonize 100 nM CP55940-induced inhibition of cAMP in F2.61A mutant while preserving their potencies in F2.61W mutant (mutations were on hCB1, and functional assays were done in stably transfected CHO cells) [6]. Also, CP55940 displayed similar potency in both F2.61A and F2.61W in inhibition of cAMP compared to the hCB1 WT stably transfected in CHO cells, [8] while the binding affinities for CP55940, HU210, and Δ^9 -THC determined against [3 H]SR141716A were severely affected by F2.61A mutation transiently transfected in HEK293 cells [45]. In the same study, the potency of HU210 in inducing [35 S]GTP γ S binding has been reported to be 30-fold less in F2.61A hCB1 mutant compared to the WT [45].

The F2.64A mutation has also been shown to be detrimental for agonists (HU210, CP55940, and Δ^9 -THC) binding [45]. CP55940, AM841, and AM11542 displayed about an order of magnitude lower potency in inhibition of forskolin-stimulated cAMP in CHO cells expressing the mutant receptor [8]. In crystal structures, this residue forms major contacts with the agonists' (C-ring, **Figure 2**) [8], and does not display any contact with the antagonists due to the presence of the N-terminus [6, 7], and no mutation data are available to characterize antagonists binding or potency in this mutant.

4.5.2. F3.25

Different studies determined binding affinity of CP55940 to F3.25A mutant; in one study, the binding affinity of CP55940 determined by saturation binding against [3 H]SR141716A was 60-fold lower in F3.25A hCB1 stably transfected in CHO-K1 cells compared to WT [38]. In other studies, CP55940 affinity was not affected in F3.25A mCB1 mutant receptor stably transfected into HEK293 cells, affinity was determined using [3 H]CP55940 [16, 46]. The discrepancy in binding affinities here could be due to species differences. F3.25A did not affect SR141616A binding in those studies [16, 38, 46]. Basal [35 S]GTP γ S binding was also determined for the F3.25A mCB1 mutant stably transfected in HEK293 cells and was not significant from WT, while the WIN55212-2 induced [35 S]GTP γ S binding was lower in the mutant with EC_{50} value

being 6-fold higher compared to the WT. In crystal structures, this residue shows moderate VDW interactions with the crystallized agonists (C-ring, **Figure 2**) [8], and no direct interactions with the antagonists [6, 7].

4.5.3. Y5.39, W5.43

Y5.39 is a conserved residue in many class A GPCRs. In the active state crystal structures, Y5.39 interacts with the agonists and forms a hydrogen bond interaction with the isothiocyanate moiety in AM841. Mutation data published along with the crystal structures show that mutation of this residue in hCB1 into phenylalanine or alanine results in significant reduction in the potencies of CP55940, AM841, and AM11542 in the inhibition of forskolin-induced cAMP, with pEC_{50} values for CP55940 being 8.3 ± 0.15 for the WT and 6.7 ± 0.13 and 5.4 ± 0.95 for the Y5.39F and Y5.39A mutants respectively [8]. Efficacy data for CP55940 are consistent with previous report from Abood's Lab [47]. In this report, WIN55212-2 has been shown to retain its WT potency in the Y5.39F mutant. In addition, the Y5.39F hCB1 mutant generally retained WT binding affinities for CP55940, Δ^9 -THC, WIN55212-2, and SR141716A and resulted in 17-fold lower K_i value for anandamide. On the other hand, Y5.39I hCB1 mutant resulted in loss of ligand binding. Authors concluded that aromaticity is required at this position [47]. Results from Abood's lab suggest that aromaticity is required for ligand binding generally, while the phenolic ring is required for signal transduction for classical and non-classical cannabinoids.

The W5.43A mutation in mCB1 was detrimental for the binding of SR141716A [16, 46], this mutation also negatively affected the binding affinity of AM251 to the mutant hCB1 with 54-fold lower affinity, while it resulted in only 7-fold lower affinity for taranabant [32]. This mutant resulted in 16-fold reduction in affinity of WIN55212-2, but did not affect either CP55940 or anandamide binding [16, 46]. The potency of CP55940 in stimulation of $[^{35}\text{S}]\text{GTP}\gamma\text{S}$, however, was 66-fold lower in the mutant receptor compared to the WT, while the basal $[^{35}\text{S}]\text{GTP}\gamma\text{S}$ binding for the W5.43A mutant being comparable to WT [46]. In active state crystal structures, this residue forms strong VDW interaction with AM841 and AM11542 aliphatic tails. In inactive state structures, the residue forms moderate VDW interactions with the 4-chlorophenyl ring in taranabant and the aliphatic chain-substituted phenyl ring in AM6538, an interaction that is inconsistent with the mutation data which suggests that W5.43 stabilizes the binding site of the antagonists, rather than being a strong interaction site with the antagonists.

4.5.4. W6.48, F3.36: the rotamer toggle switch

W6.48 belongs to the conserved CWXP hinge motif in TMH6. A W6.48 χ_1 rotameric state change from g+ to trans has been proposed to be the binding pocket trigger for the hinge motion of TMH6 that occurs during receptor activation. Here the IC end of TMH6 moves away from the TMH bundle, providing an opening into which the alpha-5 helix of the G-protein can insert [48–52]. This rotameric change is manifest for class A GPCRs in Molecular Dynamics (MD) simulations [18, 53–55], even though available active state crystal structures of class A GPCRs do not show evidence for this rotameric change. The W6.48A mCB1 mutation resulted in a 7-fold increase in binding affinity (K_i) of SR141716A compared to the WT receptor, while it had no effect on the dissociation constant of CP55940 [16, 46]. In the CB1 crystal structures, only antagonists show mild VDW interaction with W6.48.

Computational modeling and mutation studies targeting F3.36 in CB1 receptor suggested that the F3.36/W6.48 interaction represents a toggle switch that stabilizes the inactive state of the receptor [46, 56]. Consistent with the inactive and active state CB1 crystal structures, the modeling study suggested that F3.36/W6.48 contact is broken during activation with a rotameric change of the χ_1 dihedral of F3.36 from trans in the inactive state to g+ upon activation. The F3.36A CB1 mutation resulted in increased basal signaling of the receptor and did not affect the CP55940 dissociation constant, but reduced the binding affinity of SR141716A [16, 46, 57, 58]. An F3.36L mutation generally restored the binding affinity of SR141716A to the receptor [57]. In a different study, the F3.36L mutation resulted in a 7- and 9-fold lower binding affinities for taranabant and AM251 respectively [32]. In the CB1 crystal structures, only agonists show mild VDW interaction with F3.36 via their dimethyl substituent. Thus, the reduction in the binding affinity of SR141716A to the F3.36A mutant could be a result of shifting the equilibrium towards active state.

While the rotameric change of F3.36 only and not W6.48 is evident in the CB1 crystal structures, it is essential to notice that this change requires a synchronized rotameric change in the χ_1 , as well as, the χ_2 dihedrals of W6.48. Thus, it could be proposed that a transient rotameric change in χ_1 dihedral of W6.48 from g+ to trans or vice-versa is required to permit conformational changes in F3.36. In addition, the major rotameric change in F3.36 is associated with a rotational movement of TMH3 towards TMH2. Agonists appear to stabilize this conformational change in TMH3 by blocking F3.36 in g+, thus stabilizing the active state of the receptor. While in the inactive state structures, it could be noticed that the antagonists seem to prohibit the rotameric change of W6.48 into trans, thus acting as inverse agonists at the CB1 receptor.

4.5.5. F7.35

This residue has been shown to mildly affect SR141716A binding with ~4-fold increase in K_d in F7.35A hCB1 mutant [44]. Potencies of SR141716A and AM6538 in inhibiting 100 nM CP55940 activity were also retained in F7.35A and F7.35W hCB1 mutations [6]. However, the potency of CP55940, AM841, and AM11542 in inhibition of forskolin-induced cAMP has been shown to be around one order of magnitude affected by F7.35W mutation which might be due to steric hindrance, while their potencies were majorly affected by a F7.35A mutation [6, 8]. This residue shows moderate VDW interactions with the gem dimethyl group at C1' of agonists and very mild VDW interactions with the antagonists in the active and inactive state crystal structures respectively.

4.6. EC2 loop residues

The CB1 EC2 loop lines the binding site with five amino acid residues residing on top of the ligand binding site; 267-IFPHI-271. Mutations at the EC2 loop have been shown to affect CP55940 binding generally and have no effect on SR141716A binding. Replacement of the entire hCB1 EC2 loop (254-GWNCEKLQSVCSDFPHIDETYL-276) by the hCB2 EC2 loop (GWTCCPRP - - CSELFPLIPNDYL) did not affect SR141716A binding but resulted in a complete loss of CP55940 binding, while replacing EKLQSV in CB1 by CPRP (CB2/EC2) resulted in receptor sequestration [41]. In addition, the C257/C264 internal disulfide bridge has been determined to be required for membrane expression [41, 59]. Single point alanine mutations

were investigated for the majority of the EC2 loop. Among the residues that face the binding site, F268A/N hCB1 mutation impaired receptor membrane expression. F268Y hCB1 mutation had no effect on ligand binding, while F268W mutation drastically affected CP55940 binding with no effect on SR141716A binding. In addition, P267A, H270A, and I271A mutants showed no effect on SR141716A binding while drastically affecting CP55940 binding [60]. In crystal structures, F268 forms strong VDW interaction with both agonists and antagonists in addition to an aromatic stacking with the agonists. P267 and I271 form weak VDW interaction with agonists while the H270 side chain points towards TMH3 and is packed against F3.25. In addition, due to closer packing of the EC end of TMH5/6 towards the ligand binding site in the active state compared to the inactive state, and the fact that agonists are cupping F268 compared to the antagonists, it could be interpreted that F268W mutation data regarding the binding of agonists versus the antagonists could be consistent with crystal structures.

4.7. Cysteine residues in the EC domain of CB1; labeling and mutation studies

Among the 13 cysteine residues in the CB1 receptor, C6.47, C7.38, and C7.42 reside in the EC transmembrane domain and are not engaged in a disulfide bond. C6.47 is only available in the binding pocket in the activated state of Class A GPCRs. Consistent with this, the earliest CB1 cysteine reactivity study using the isothiocyanate derivatized agonist, AM841, showed that AM841 labels C6.47 [61]. A subsequent study showed that AM841 also labels C6.47 in CB2 [62]. The isothiocyanate derivatized anandamide analog, AM3677, was also found to label C6.47 [63]. This has led to the hypothesis that cannabinoid agonists enter CB1 via a portal between TMH6 and TMH7 at the level of C6.47. The active state crystal structure, is not consistent with cysteine crosslinking studies of AM841, since the AM841 alkyl tail points towards Y5.39 in the crystal structure.

In another cysteine reactivity study, C7.42, was found reactive, suggesting that it faces the binding pocket. Mutation of C7.42 to a larger amino acid resulted in loss of SR141716A binding, but not CP55940 binding. In all reported crystal structures, C7.42 faces into the binding pocket. Further, if C7.42 is mutated to M in the active state structure, it does not affect the agonist binding pocket. However, a methionine residue at that position in the inactive state structures clashes severely with the antagonists and surrounding residues, such clashes are not relieved by rotameric changes for nearby residues.

4.8. Serine residues in CB1

Mutation of S7.39 in hCB1 to alanine in was generally detrimental for CP55940, HU201 and AM4056 binding to the CB1 receptor, while it had no effect on the binding affinities for SR141716A, AM251, as well as, WIN55212 [32, 57, 64]. On the other hand, it resulted in a profound reduction in the binding affinity of taranabant to the receptor [32]. In the inactive state crystal structure in complex with taranabant, as well as, the active state crystal structure, there is a hydrogen bond interaction between S7.39 and the ligand. The residue adopts a $g^- \chi_1$ dihedral that allows this interaction. In the AM6358/inactive state crystal structure, this residue adopts a $g^+ \chi_1$ dihedral. In this structure, the ligand is incapable of forming a hydrogen bond interaction with S7.39, since such an interaction requires a high energy conformation of the antagonist.

Mutation data show that the S2.60A mutation in hCB1 has no effect on the binding affinities of both CP55940 and SR141716A [64]. S2.60 does not seem to be involved in any interactions with ligands in the crystal structures. This is due to the rotation of TMH2 towards TMH3 caused by the G2.53/S2.54 motif in TMH2 allowing a wider turn in that region.

4.9. L3.29A, M6.55A, and T3.33A mutations

L3.29 faces the ligand binding site and has been shown to interact with both agonists and antagonists. Such interactions are stronger in the active state due to the rotation of TMH3 towards TMH2, allowing L3.29 to be more oriented towards the binding site. The L3.29A mutation in hCB1 has been shown to mildly affect the binding affinity of SR141716A to the receptor, while having a profound effect on the binding of CP55940, HU210 and Δ^9 -THC. The L3.29A mutations resulted in reduced efficacy of both HU210 in stimulation of [35 S]GTP γ S binding and in the efficacy of CP55940 in the inhibition of forskolin-induced cAMP accumulation [8, 44, 45].

Both T3.33A and M6.55A mutations did not have any effect on the binding affinity of SR141716A which is consistent with the inactive state crystal structures [44]. M6.55A mutation in hCB1 resulted in a 15- and 4-fold reduction in the affinity of HU210 and CP55940 respectively while it did not affect the affinity of Δ^9 -THC [45]. This residue shows moderate VDW interactions with the agonists in the crystal structures.

5. NMR and circular dichroism (CD) studies on the C-terminus

Both NMR and CD studies have been performed on the C-terminus of CB1 employing peptide segments that correspond to that receptor region. Results show a helical segment resembling helix 8 that is parallel to the plane of the membrane [65–67]. Ahn et al., reported two amphipathic α -helical domains; S410-F412 that corresponds to helix 8, and a second helical segment (A440-M461) that is also parallel to the membrane, (**Figure 1**) [65].

6. Crystal contacts

In the inactive and active state CB1 crystal structures, crystal packing impinges on the ligand binding site (**Figure 6**). In the first published CB1 inactive state structure [6], receptor bundles are crystallized top-to-top, forcing the N-terminus to invade the binding pocket and flattening the EC loops. In the second inactive state CB1 structure [7], adjacent bundles impinge on receptor EC loops and N-terminus around the “rim” of the receptor’s EC domain (**Figure 6**). The effect on CB1 structure is similar to that discussed above for the first inactive crystal structure. Crystal packing in the active state structure [8] also causes an impact on the CB1 binding pocket. Packing causes TMH2 to hinge at G2.53/S2.54 (S2.54 has a $\chi_1 = g^-$) and invade the binding pocket. Packing also impacts the N-terminus, TMH1 above N1.50, the EC top of TMH3, the EC-2 loop and the EC end of TMH4.

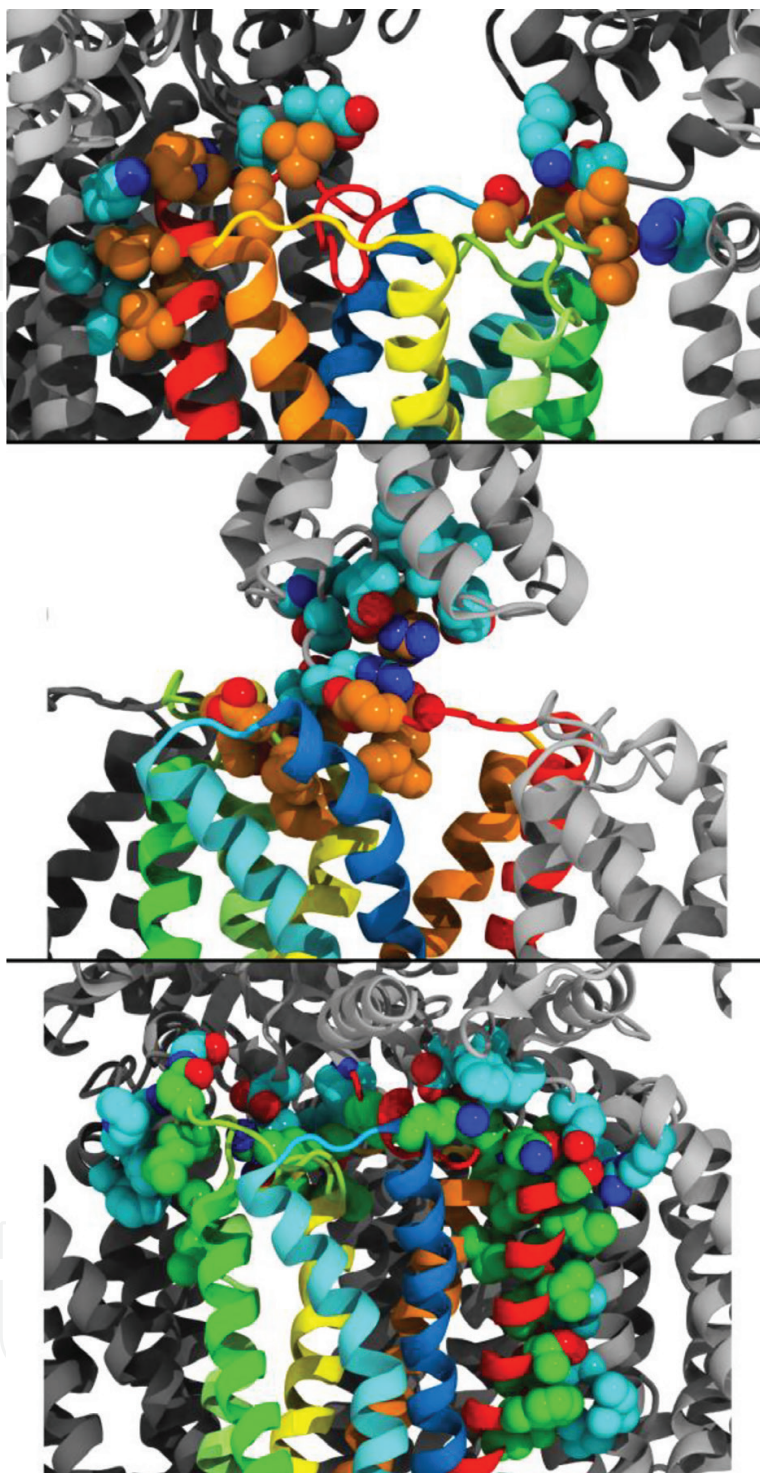


Figure 6. Unit cell TM region and extracellular loop crystal contacts for hCB1 receptor crystal structures. CB1 ribbon colors: TMH1 (red), TMH2 (orange), TMH3 (yellow), TMH4 (pale green), TMH5 (green), TMH6 (cyan), TMH7 (blue), crystal mate ribbons (white). Top panel: inactive state structure (PDB ID: 5TGZ) [6]. Middle panel: inactive state structure (PDB ID: 5U09) [7]. Bottom panel: active state structure (PDB ID: 5XRA) [8]. Amino acid residues for crystal mates are colored cyan, while inactive and active state structures are shown in orange and green respectively.

Such packing issues can promote non-genuine conformations in the structure that is promoted by the crystalline low energy state. A recently published crystal structure of the μ -opioid receptor (MOR) has revealed a histidine H54 residue in the N-terminus of the receptor that

is positioned 2.6 Å from the secondary amine of the bound agonist. Mutation of this residue into alanine did not affect the affinity of the ligand to the receptor, suggesting that the resulting conformation of the N-terminus in MOR structure is a result of crystallization and not relevant in the real state [68].

7. Conclusions

Because X-ray crystal structures are used frequently for drug design projects, it is critical to identify any issues with these structures, such as crystal packing effects and to evaluate how consistent these structures are with the body of structural information in the literature for a given receptor, such as mutation, cross-linking and NMR studies. Results presented in this chapter show that crystal packing issues impact both of the CB1 inactive state crystal structures and the activated state CB1 crystal structures. Impacts include N-terminus insertions deep into the binding pocket seen in the CB1 inactive state structures, as well as, TMH1 and TMH2 bending into the binding pocket seen in the activated state structures. Not surprisingly, we find here that the CB1 structures have important inconsistencies with mutation data, particularly in their TMH1-2-3 regions. In addition, the CB1 crystal structures do not capture the movement of W6.48 during receptor activation, or the existence of a ligand portal in the activated state, however, X-ray structures by their very nature will not capture all transient changes. In conclusion, then, the CB1 crystal structures are an important contribution to the drug design field, but revisions are advisable before these structures are used for structure-based drug discovery.

Acknowledgements

This work was supported by NIDA RO1 DA003934 to PHR.

Author details

Rufaida Al-Zoubi¹, Dow P. Hurst² and Patricia H. Reggio^{2*}

*Address all correspondence to: phreggio@uncg.edu

¹ Department of Medicinal Chemistry and Pharmacognosy, Faculty of Pharmacy, Jordan University of Science and Technology, Irbid, Jordan

² Department of Chemistry and Biochemistry, University of North Carolina at Greensboro, Greensboro, NC, USA

References

- [1] Palczewski K et al. Crystal structure of rhodopsin: A G protein-coupled receptor. *Science*. 2000;**289**(5480):739

- [2] Jaakola V-P et al. The 2.6 angstrom crystal structure of a human A2A adenosine receptor bound to an antagonist. *Science*. 2008;**322**(5905):1211-1217
- [3] Warne T et al. Structure of a β 1-adrenergic G-protein-coupled receptor. *Nature*. 2008;**454**:486
- [4] Hanson MA et al. A specific cholesterol binding site is established by the 2.8 Å structure of the human beta2 adrenergic receptor. *Structure*. 2008;**16**(6):897-905
- [5] Scheerer P et al. Crystal structure of opsin in its G-protein-interacting conformation. *Nature*. 2008;**455**:497
- [6] Hua T et al. Crystal structure of the human cannabinoid receptor CB1. *Cell*. 2016;**167**(3):750-762.e14
- [7] Shao Z et al. High-resolution crystal structure of the human CB1 cannabinoid receptor. *Nature*. 2016;**540**:602
- [8] Hua T et al. Crystal structures of agonist-bound human cannabinoid receptor CB1. *Nature*. 2017;**547**(7664):468-471
- [9] Fredriksson R et al. The G-protein-coupled receptors in the human genome form five main families. Phylogenetic analysis, Paralogon groups, and fingerprints. *Molecular Pharmacology*. 2003;**63**(6):1256-1272
- [10] Devillé J, Rey J, Chabbert M. An indel in transmembrane helix 2 helps to trace the molecular evolution of class A G-protein-coupled receptors. *Journal of Molecular Evolution*. 2009;**68**(5):475-489
- [11] Pel J et al. Multidimensional scaling reveals the main evolutionary pathways of class A G-protein-coupled receptors. *PLoS One*. 2011;**6**(4):1-10
- [12] Surgand JS et al. A chemogenomic analysis of the transmembrane binding cavity of human G-protein-coupled receptors. *Proteins: Structure, Function and Genetics*. 2006;**62**(2):509-538
- [13] Chrencik JE et al. Crystal structure of antagonist bound human lysophosphatidic acid receptor 1. *Cell*. 2015;**161**(7):1633-1643
- [14] Hanson MA et al. Crystal structure of a lipid G protein-coupled receptor. *Science*. 2012;**335**(6070):851
- [15] Vallée M et al. Pregnenolone can protect the brain from Cannabis intoxication. *Science*. 2014;**343**(6166):94-98
- [16] McAllister SD et al. An aromatic microdomain at the cannabinoid CB1 receptor constitutes an agonist/inverse agonist binding region. *Journal of Medicinal Chemistry*. 2003;**46**(24):5139-5152
- [17] Stanley N, Pardo L, Fabritiis GD. The pathway of ligand entry from the membrane bilayer to a lipid G protein-coupled receptor. *Scientific Reports*. 2016;**6**:22639
- [18] Hurst DP et al. A lipid pathway for ligand binding is necessary for a cannabinoid G protein-coupled receptor. *Journal of Biological Chemistry*. 2010;**285**(23):17954-17964

- [19] Venkatakrisnan AJ et al. Diverse activation pathways in class A GPCRs converge near the G-protein-coupling region. *Nature*. 2016;**536**:484
- [20] Carpenter B, Tate CG. Active state structures of G protein-coupled receptors highlight the similarities and differences in the G protein and arrestin coupling interfaces. *Current Opinion in Structural Biology*. 2017;**45**:124-132
- [21] Bonner TI, Song ZH. A lysine residue of the cannabinoid receptor is critical for receptor recognition by several agonists but not WIN55212-2. *Molecular Pharmacology*. 1996;**49**(5):891-896
- [22] Chin CN et al. Ligand binding and modulation of cyclic AMP levels depend on the chemical nature of residue 192 of the human cannabinoid receptor 1. *Journal of Neurochemistry*. 1998;**70**(1):366-373
- [23] Shore DM et al. Allosteric modulation of a cannabinoid G protein-coupled receptor: Binding site elucidation and relationship to G protein signaling. *Journal of Biological Chemistry*. 2014;**289**(9):5828-5845
- [24] Tuccinardi T et al. Cannabinoid CB2/CB1 selectivity. Receptor modeling and automated docking analysis. *Journal of Medicinal Chemistry*. 2006;**49**(3):984-994
- [25] Salo OMH et al. 3D-QSAR studies on cannabinoid CB1 receptor agonists: G-protein activation as biological data. *Journal of Medicinal Chemistry*. 2006;**49**(2):554-566
- [26] Salo OMH et al. Development of a 3D model for the human cannabinoid CB1 receptor. *Journal of Medicinal Chemistry*. 2004;**47**(12):3048-3057
- [27] Shim JY, Welsh William J, Howlett Allyn C. Homology model of the CB1 cannabinoid receptor: Sites critical for nonclassical cannabinoid agonist interaction. *Peptide Science*. 2004;**71**(2):169-189
- [28] Joong-Youn S. Understanding functional residues of the cannabinoid CB1 receptor for drug discovery. *Current Topics in Medicinal Chemistry*. 2010;**10**(8):779-798
- [29] Hurst DP et al. N-(piperidin-1-yl)-5-(4-chlorophenyl)-1-(2,4-dichlorophenyl)-4-methyl-1H-pyrazole-3-carboxamide (SR141716A) interaction with LYS 3.28(192) is crucial for its inverse agonism at the cannabinoid CB1 receptor. *Molecular Pharmacology*. 2002;**62**(6):1274-1287
- [30] Pan X, Ikeda SR, Lewis DL. SR 141716A acts as an inverse agonist to increase neuronal voltage-dependent Ca²⁺ currents by reversal of tonic CB1 cannabinoid receptor activity. *Molecular Pharmacology*. 1998;**1072**:1064-1072
- [31] Hurst D et al. Biarylpyrazole inverse agonists at the cannabinoid CB1 receptor: Importance of the C-3 Carboxamide oxygen/lysine 3.28(192) interaction. *Journal of Medicinal Chemistry*. 2006;**49**(20):5969-5987
- [32] Lin LS et al. Conformational analysis and receptor docking of N-[(1S,2S)-3-(4-chlorophenyl)-2-(3-cy-anophenyl)-1-methylpropyl]-2-methyl-2- \ \{[5-(trifluoromethyl)pyridin-2-yl]oxy} propanamide (Taranabant, MK-0364), a novel , acyclic canna. *Journal of Medicinal Chemistry*. 2008;**51**:2108-2114

- [33] Fong TM et al. Antiobesity efficacy of a novel cannabinoid-1 receptor inverse agonist, N-[(1S,2S)-3-(4-chlorophenyl)-2-(3-cyanophenyl)-1-methylpropyl]-2-methyl-2-[[5-(trifluoromethyl)pyridin-2-yl]oxy] propanamide (MK-0364), in rodents. *Journal of Pharmacology and Experimental Therapeutics*. 2007;**321**(3):1013
- [34] Ahn KH et al. Computationally-predicted CB1 cannabinoid receptor mutants show distinct patterns of salt-bridges that correlate with their level of constitutive activity reflected in G protein coupling levels, thermal stability, and ligand binding. *Proteins*. 2013;**81**(8):1304-1317
- [35] Kapur A et al. Mapping the structural requirements in the CB1 cannabinoid receptor transmembrane Helix II for signal transduction. *Journal of Pharmacology and Experimental Therapeutics*. 2008;**325**(1):341-348
- [36] D'Antona AM et al. A cannabinoid receptor 1 mutation proximal to the DRY motif results in constitutive activity and reveals intramolecular interactions involved in receptor activation. *Brain Research*. 2006;**1108**(1):1-11
- [37] Marcu J et al. Novel insights into CB1 cannabinoid receptor signaling: A key interaction identified between the extracellular-3 loop and transmembrane helix 2. *The Journal of Pharmacology and Experimental Therapeutics*. 2013;**345**(2):189-197
- [38] Murphy JW, Kendall DA. Integrity of extracellular loop 1 of the human cannabinoid receptor 1 is critical for high-affinity binding of the ligand CP 55,940 but not SR 141716A. *Biochemical Pharmacology*. 2003;**65**(10):1623-1631
- [39] Fay JF, Farrens DL. The membrane proximal region of the cannabinoid receptor CB1 N-terminus can Allosterically modulate ligand affinity. *Biochemistry*. 2013;**52**(46):8286-8294
- [40] Andersson H et al. Membrane assembly of the cannabinoid receptor 1: Impact of a long N-terminal tail. *Molecular Pharmacology*. 2003;**64**(3):570
- [41] Shire D et al. Structural features of the central cannabinoid CB1 receptor involved in the binding of the specific CB1 antagonist SR 141716A. *Journal of Biological Chemistry*. 1996;**271**(12):6941-6946
- [42] Iyer MR et al. Structural basis of species-dependent differential affinity of 6-alkoxy-5-aryl-3-pyridinecarboxamide cannabinoid receptor 1 antagonists running title: Species-specific affinity of CB1 receptor antagonists. *Molecular Pharmacology*. 2015;**88**(2):238-244
- [43] Rover S et al. 6-Alkoxy-5-aryl-3-pyridinecarboxamides, a new series of bioavailable cannabinoid receptor type 1 (CB1) antagonists including peripherally selective compounds. *Journal of Medicinal Chemistry*. 2013;**56**(24):9874-9896
- [44] Shim JY, Bertalovitz AC, Kendall DA. Probing the interaction of SR141716A with the CB1 receptor. *Journal of Biological Chemistry*. 2012;**287**(46):38741-38754
- [45] Shim J-Y, Bertalovitz AC, Kendall DA. Identification of essential cannabinoid-binding domains: Structural insights into early dynamic events in receptor activation. *Journal of Biological Chemistry*. 2011;**286**(38):33422-33435

- [46] McAllister SD et al. Structural mimicry in class A G protein-coupled receptor rotamer toggle switches: The Importance of the F3.36(201)/W6.48(357) interaction in cannabinoid CB1 receptor activation. *Journal of Biological Chemistry*. 2004;**279**(46):48024-48037
- [47] McAllister SD et al. A critical role for a tyrosine residue in the cannabinoid receptors for ligand recognition. *Biochemical Pharmacology*. 2002;**63**(12):2121-2136
- [48] Klein-Seetharaman J et al. Differential dynamics in the G protein-coupled receptor rhodopsin revealed by solution NMR. *Proceedings of the National Academy of Sciences of the United States of America*. 2004;**101**(10):3409-3413
- [49] Holst B et al. A conserved aromatic lock for the tryptophan rotameric switch in TM-VI of seven-transmembrane receptors. *Journal of Biological Chemistry*. 2010;**285**(6):3973-3985
- [50] Lin SW, Sakmar TP. Specific tryptophan UV-absorbance changes are probes of the transition of rhodopsin to its active state. *Biochemistry*. 1996;**35**(34):11149-11159
- [51] Borhan B et al. Movement of retinal along the visual transduction path. *Science*. 2000;**288**(5474):2209-2212
- [52] Trzaskowski B et al. Action of molecular switches in GPCRs—Theoretical and experimental studies. *Current Medicinal Chemistry*. 2012;**19**(8):1090-1109
- [53] Yuan S et al. Activation of G-protein-coupled receptors correlates with the formation of a continuous internal water pathway. *Nature Communications*. 2014;**5**(May):4733-4733
- [54] Yuan S, Vogel H, Filipek S. The role of water and sodium ions in the activation of the μ -opioid receptor. *Angewandte Chemie—International Edition*. 2013;**52**(38):10112-10115
- [55] Nygaard R et al. Conserved water-mediated hydrogen bond network between TM-I, -II, -VI, and -VII in 7TM receptor activation. *Journal of Biological Chemistry*. 2010;**285**(25):19625-19636
- [56] Singh R et al. Activation of the cannabinoid CB1 receptor may involve a W6.48/F3.36 rotamer toggle switch. *The Journal of Peptide Research*. 2002;**60**(6):357-370
- [57] Sitkoff DF et al. Cannabinoid CB1 receptor ligand binding and function examined through mutagenesis studies of F200 and S383. *European Journal of Pharmacology*. 2011;**651**(1):9-17
- [58] Shen C-P et al. F200A substitution in the third transmembrane helix of human cannabinoid CB1 receptor converts AM2233 from receptor agonist to inverse agonist. *European Journal of Pharmacology*. 2006;**531**(1):41-46
- [59] Fay JF, Dunham TD, Farrens DL. Cysteine residues in the human cannabinoid receptor: Only C257 and C264 are required for a functional receptor, and steric bulk at C386 impairs antagonist SR141716A binding. *Biochemistry*. 2005;**44**(24):8757-8769
- [60] Ahn KH et al. Dual role of the second extracellular loop of the cannabinoid receptor 1: Ligand binding and receptor localization. *Molecular Pharmacology*. 2009;**76**(4):833-842

- [61] Picone RP et al. (-)-7'-Isothiocyanato-11-hydroxy-1',1'-dimethylheptylhexahydrocannabinol (AM841), a high-affinity electrophilic ligand, interacts covalently with a cysteine in Helix six and activates the CB1 cannabinoid receptor. *Molecular Pharmacology*. 2005; **68**(6):1623-1635
- [62] Pei Y et al. Ligand-binding architecture of human CB2 cannabinoid receptor: Evidence for receptor subtype-specific binding motif and modeling GPCR activation. *Chemistry & Biology*. 2008; **15**(11):1207-1219
- [63] Janero DR et al. Molecular-interaction and signaling profiles of AM3677, a novel covalent agonist selective for the cannabinoid 1 receptor. *ACS Chemical Neuroscience*. 2015; **6**(8): 1400-1410
- [64] Kapur A et al. Mutation studies of Ser7.39 and Ser2.60 in the human CB1 cannabinoid receptor: Evidence for a serine-induced bend in CB1 transmembrane Helix 7. *Molecular Pharmacology*. 2007; **71**(6):1512
- [65] Ahn KH et al. Structural analysis of the human cannabinoid receptor one carboxyl-terminus identifies two amphipathic helices. *Biopolymers*. 2009; **91**(7):565-573
- [66] Choi G, Guo J, Makriyannis A. The conformation of the cytoplasmic helix 8 of the CB1 cannabinoid receptor using NMR and circular dichroism. *Biochimica et Biophysica Acta (BBA)—Biomembranes*. 2005; **1668**(1):1-9
- [67] Tyukhtenko S et al. NMR solution structure of human cannabinoid receptor-1 helix 7/8 peptide: Candidate electrostatic interactions and microdomain formation. *Biochemical and Biophysical Research Communications*. 2009; **390**(3):441-446
- [68] Huang W et al. Structural insights into μ -opioid receptor activation. *Nature*. 2015; **524**:315